Structural Variations in Carboxylated Bispidine Ligands: Influence of Positional Isomerism and Rigidity on the Conformation, Stability, Inertness and Relaxivity of their Mn 2+ Complexes

Daouda Ndiaye, Maryame Sy, Waygen Thor, Loïc Charbonnière, Aline Nonat, Éva Tóth

Structural variations in carboxylated bispidine ligands: influence of positional isomerism and rigidity on the conformation, stability, inertness and relaxivity of their Mn^{2+} complexes

Daouda Ndiaye,[a]‡ Maryame Sy,[b]‡, Waygen Thor,[b] Loïc J. Charbonnière,[b]* Aline M. Nonat,[b]* and Éva Tóth[a]*

[a] Dr Éva Tóth, Dr Daouda Ndiaye
Centre de Biophysique Moléculaire
CNRS UPR 4301, Université d'Orléans
Rue Charles Sadron, F-45071 Orléans
E-mail: eva.jakabtoth@cnrs-orleans.fr

[b] Dr Aline Nonat, Dr Loïc Charbonnière, Dr Maryame Sy, Waygen Thor
Equipe de Synthèse pour l'Analyse, Département des Sciences Analytiques
Université de Strasbourg, CNRS, IPHC UMR 7178
27, Rue Becquerel, F-67A037 Strasbourg
E-mail: aline.nonat@unistra.fr; l.charbonn@unistra.fr

Supporting information for this article is given via a link at the end of the document.

Abstract: Mn^{2+} complexes of 2,4-pyridyl-disubstituted bispidine ligands have emerged as more biocompatible alternatives to Gd^{3+}-based MRI probes. They display relaxivities comparable to that of commercial contrast agents and high kinetic inertness, unprecedented for Mn^{2+} complexes. The chemical structure, in particular the substituents on the two macrocyclic nitrogens N3 and N7, are decisive for the conformation of the Mn^{2+} complexes, and this will in turn determine their thermodynamic, kinetic and relaxation properties. We describe the synthesis of four ligands with acetate substituents in positions N3, N7 or both. We evidence that the bispidine conformation is dependent on N3 substitution, with direct impact on the thermodynamic stability, kinetic inertness, hydration state and relaxivity of the Mn^{2+} complexes. These results unambiguously show that (i) solely a chair-chair conformation allows for favorable inertness and relaxivity, and (ii) in this family such chair-chair conformation is accessible only for ligands without N3-appended carboxylates.

Introduction

Mn^{2+} complexes meet increasing interest in the context of imaging applications. This is largely promoted by the search for safer alternatives to current gadolinium (Gd) based magnetic resonance imaging (MRI) contrast media, following recent toxicity concerns related to Gd[1] and the observation of Gd-deposition in different organs.[2] Mn^{2+}, Mn^{3+} and Fe^{3+} are the most obvious paramagnetic transition metal ion candidates to replace Gd^{3+}.[3] In particular, manganese is an essential metal,[4] and in its high-spin 2+ oxidation state, it is a powerful relaxation agent.[5] There is also interest in manganese beyond MRI as ^{52}Mn is an emerging radionuclide for positron emission tomography (PET)[6] ($t_{1/2}$ = 5.6 d, max. β^+-energy: 575 keV). Its low β^+ decay intensity (29.6%) allows good spatial resolution and the long $t_{1/2}$ makes ^{52}Mn adapted to image slow biological processes. Mn^{2+} is the unique metal ion that offers detection in both MRI and PET.

For *in vivo* imaging applications, Mn^{2+} complexes must be stable and inert to prevent free metal release in the body, which could be harmful at the elevated concentrations needed for MRI and would cause undesirable off-target signals in PET.[7] In addition, for MRI, the chelates must also have good relaxivity, which requires at least one inner sphere water molecule. Due to the d^5 electronic configuration and the lack of crystal field stabilization energy for the high-spin Mn^{2+} state, high thermodynamic stability as well as kinetic inertness are difficult to attain.[8]

During the last years, numerous linear and macrocyclic chelators have been explored for Mn^{2+} complexation. PyC3A and its derivatives represent promising examples of acyclic ligands,[9] while in the macrocyclic family, PC2A-[10] and DO2A-type[11] Mn^{2+} complexes look particularly attractive (Scheme 1). Several of these have been successfully tested in preclinical imaging and MnPyC3A has entered clinical trials.[12] In parallel to these advances, it remains important to extend the investigations to novel types of ligand structures which could grant considerable improvement in the thermodynamic stability and the kinetic inertness of Mn^{2+} complexes.

Indeed, recent findings on Mn^{2+} chelates based on bispidine ((3,7-diazabicyclo[3.3.1]nonane) have fundamentally changed our vision on stability and inertness. These highly rigid and preorganized ligands[13] provide unprecedented coordination properties for Mn^{2+}. For the monohydrated, hexadentate MnBisp1 chelate (Scheme 1), no dissociation at all was observed over a period of 130 days at pH 6, 37 °C, in the presence of 50 equiv. of Zn^{2+},[14] whereas under these similar conditions, MnPC2A-EA and MnPC2A-DPA, considered as the most inert non-bispidine Mn^{2+} chelates, have half-lives of 54.4 h[10b] and 64.5 h,[10a] respectively. Other pentadentate derivatives, such as Bisp2 allow for similarly remarkable resistance to dissociation of their monohydrated Mn^{2+} complexes.[15]

On the other hand, the hepta- and octadentate bispidine ligands Bisp3 and Bisp4 provide selectivity for Mn^{2+} over Zn^{2+}.[16] This unique property, circumventing the general Irving-Williams

rule that predicts a thermodynamic stability order of Mn^{2+} < Fe^{2+} < Co^{2+} < Ni^{2+} < Cu^{2+} > Zn^{2+} is the consequence of the enforced

a)

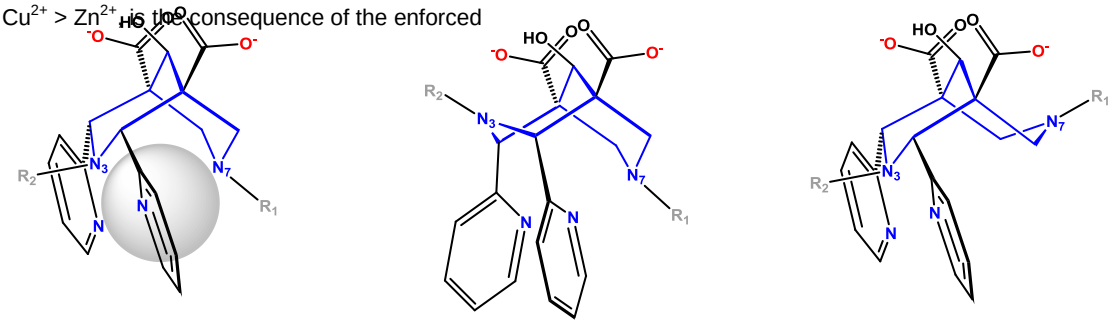

chair-chair conformation
« bicyclic cage »

boat-chair conformation

chair-boat conformation

b)

similar manner as macrocyclic cyclen (1,4,7,10-

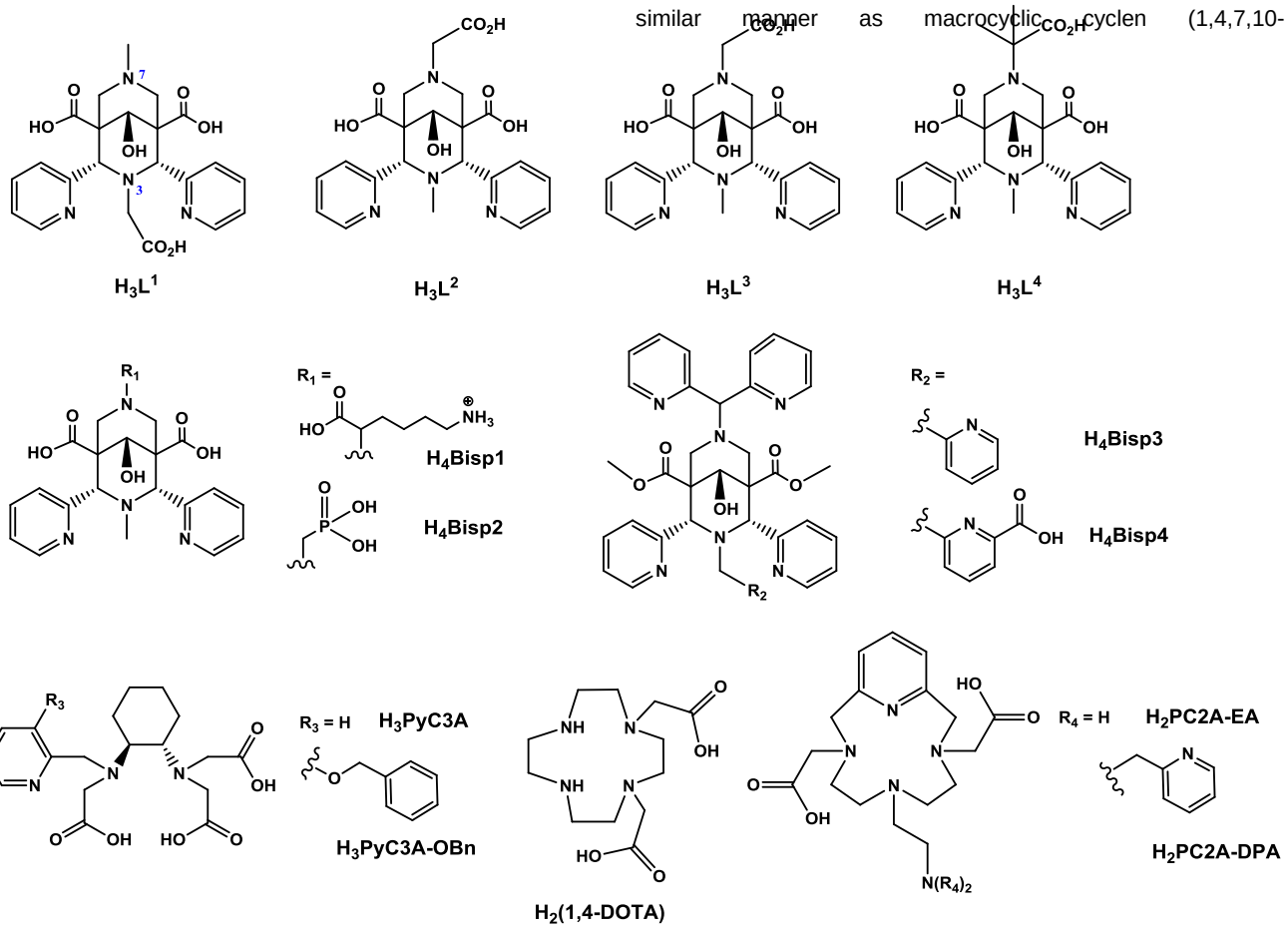

Scheme 1. Possible conformations adopted by bispidine ligands (a) and ligands discussed in this manuscript (b).

ligand rigidity, perfect size-match and full encapsulation of the Mn^{2+} ion, while Zn^{2+} is too small to accommodate all donor groups of the chelator.

Depending on the nature of substituents R_1 and R_2, respectively on the N7 and N3 nitrogens of the bicycle, and on the protonation degree of these two amines, bispidine derivatives can adopt different conformations: chair-chair (cc), boat-chair (bc) and chair-boat (cb) (Scheme 1a). The boat-boat conformation (bb) is energetically unfavorable.[17] Among these, the chair-chair conformation offers the most favorable coordination environment with a strongly pre-organized “bicyclic” cage, which is essential to obtain inert Mn^{2+} complexes, in a

tetraazacyclododecane) or macrobicyclic cryptand cages are important to provide their complexes with high kinetic inertness. Therefore, the objective of the present study was to investigate, in the family of pentadentate bispidine ligands, the influence of the nature of R_1 and R_2 groups on the bicycle conformation, and subsequently on the metal coordination properties and the physico-chemical characteristics, in particular the kinetic inertness of the Mn^{2+} complexes. Four ligands, L^1, L^2, L^3 and L^4 have been involved in this comparative study (Scheme 1b). They bear either carboxylate or methyl substituents on the N3 nitrogen (R_2), a position that turns out to be determinant for the conformation. L^1 and L^2 are positional (or constitutional) isomers, while L^3 has carboxylate functions on both N3 and N7 positions. L^2 [18] and its Mn^{2+} complex[15] have been previously reported. In addition, L^4 was synthesized to study the influence of steric crowding on the α carbon of the N7 substituent, which has previously proved to be an important element to generate higher inertness for cyclen-type lanthanide complexes.[19] To determine the conformation of the ligands and of their Zn^{2+} complexes, potentiometric titrations and NMR (ROESY) spectroscopy have been used. Then, the physico-chemical properties (thermodynamic stability, kinetic inertness, hydration number, relaxation efficacy) of the Mn^{2+} complexes have been assessed using potentiometry and ^1H and ^{17}O NMR relaxation studies. We evidence that these properties are fundamentally different when the conformation of the bispidine bicycle changes.

Results and Discussion

Synthesis

The synthesis of L^2 has been previously reported.[15] Ligands L^1,

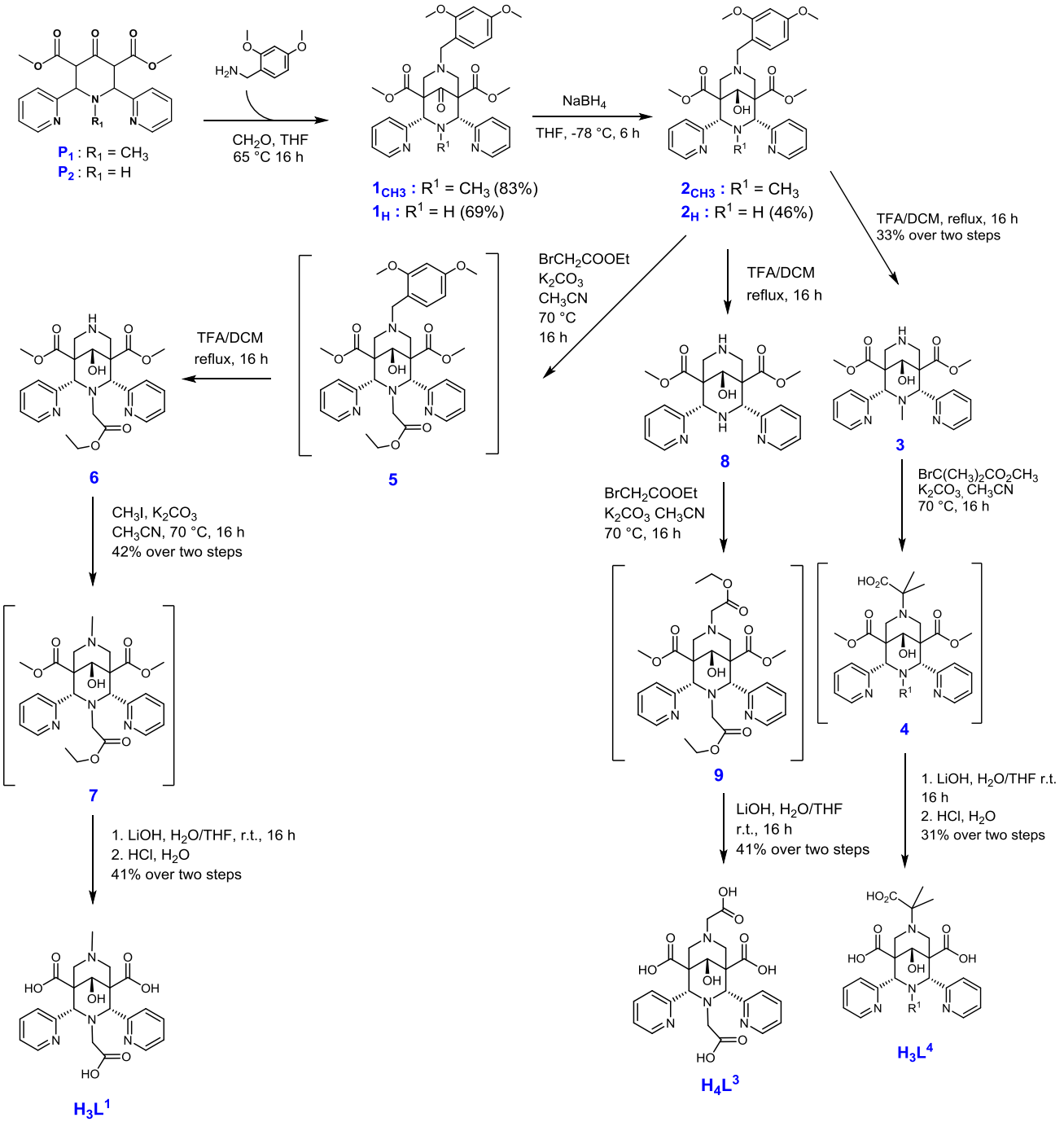

Scheme 2. Synthesis pathway for H_3L^1, H_3L^3 and H_3L^4.

L^3 and L^4 have been obtained by nucleophilic substitution of three key bispidol intermediates 2, 8 and 3,respectively, which were obtained following previously established procedures based on Mannich reactions (Scheme 2).[15, 20] After reduction of the central ketone to avoid retro-Mannich reactions, all these bispidol compounds have proton H9 pointing towards N7 as confirmed by NOESY NMR spectra (see Figure 1 for atom numbering). L^3 and L^4 were obtained in two steps, involving ethyl bromoacetate or methyl 2-bromo-2-methylpropanoate, respectively. The intermediates, possessing ester functions, were not isolated and were directly engaged in a saponification reaction with LiOH. The final ligands were purified by reverse phase chromatography (C18) to yield white powders. The final yields (41% over two steps for H_4L^3 and 31% over two steps for H_3L^4) reflect a slight influence of the substituent on the reaction kinetics and yield. For the synthesis of H_3L^1, the –DMB protected intermediate was used to selectively insert an ethylacetate substituent at N3 while maintaining the chair-chair conformation and *cis* configuration of the bispidol skeleton.[21] This intermediate was then deprotected in presence of TFA (intermediate 6) and subsequently methylated by iodomethane (intermediate 7) before saponification. The average yield for the substitution reaction with bromo ethylacetate (41% over two steps) is similar to the one of H_3L^2 or H_4L^3, indicating very minor impact of the position of the tertiary amine (N3, N7 or both) on its reactivity.

Compounds were characterized by ^{1}H- and ^{13}C-NMR, elemental analysis and ESI mass spectrometry (Figures S1-S17). ^{1}H NMR spectra were typical of bispidol-type ligands in the chair-chair or chair-boat conformation (Scheme 1) with a *cis* configuration of the pyridines and a C_S symmetry. Nevertheless, broad signals were observed for ligand L^4 which we attributed to the presence of several rotamers in solution due to the steric hindrance generated by the two methyl groups. To confirm this hypothesis, ^{1}H and ^{13}C NMR spectra of the zinc(II) complex $[ZnL^4]^-$ were measured, revealing the formation of well-resolved fine peaks characteristic of a single species in solution (Figures S15-S16).

Conformational study

Potentiometric titration of the ligands

Previous studies on bispidines have shown that the degree of protonation of the bicycle heteroatoms (protonation of either N3 or N7, or both) is intrinsically related to the conformation. The chair-chair conformation is always associated with mono-protonation of the bicycle involving the formation of a hydrogen bond between N3 and N7 amine sites which contributes to the stabilization of the molecule.[14-15, 22] On the other hand, protonation of both N3 and N7 amine nitrogens is exclusively observed in boat-chair or chair-boat conformations, which are more favorable, given the electrostatic repulsion between the positively charged amines (Scheme 1a).[23] Therefore, we have carried out pH-potentiometric titrations of the bispidine ligands L^1, L^3 and L^4 between pH 2 and 12 to determine their protonation constants. L^2 has been previously studied.[15] The analysis of these pH-potentiometric titration curves (Figure S18) yielded five logK_H values for L^1 and L^3, while four constants were obtained for L^2 and L^4 (Table 1).

Based on the protonation constant values, we distinguish two cases. For L^2 and L^4 that bear a methyl (R_2) on the N3 position, we obtain a single protonation constant in the basic pH region. Thus, the protonation constants indicate chair-chair conformation for L^2 and L^4. In contrast, for L^1 and L^3 (R_2 = acetate), two protonation constants are observed at high pH. These basic logK_H values correspond to the protonation of the amine nitrogens (N3/N7) of the bicycle (Scheme 1) and probably boat-chair or chair-boat conformation for L^1 and L^3 in acidic and neutral conditions. In addition to the electrostatic repulsion between the two positive charges, the boat-chair conformation is the most favorable since it can be further stabilized by intramolecular hydrogen bonds established between the amine proton and hydrogen acceptor sites, particularly the oxygen of the acetate (Scheme 1a).

The other protonation constants in the acidic region correspond to the different carboxylate functions. For L^3, the protonation of the third carboxylate occurs below pH ~1.8 and could not be determined from the potentiometric titration.

Further evidence on the ligand conformation has been obtained by NMR.

Table 1. Ligand protonation constants. I = 0.15 M NaCl ; 298 K. Values in parenthesis correspond to one standard deviation.

	L^1	L^2 [15]	L^3	L^4	PC2A-EA[10b]
logK_{H1}	11.37(2)	9.54	9.91(1)	10.74(1)	11.34
logK_{H2}	10.46(2)	5.11	9.05(1)	5.55(1)	8.93
logK_{H3}	4.65(3)	2.99	5.66(2)	2.89(1)	6.91
logK_{H4}	3.40(3)	1.80	3.73(2)	1.48(1)	1.97
logK_{H5}	2.89(3)	-	2.74(1)	-	-
ΣlogK_{Hi}	32.93	19.44	31.15	20.66	29.15

NMR study

To characterize the 3D structure, thus the conformation of the bispidine bicycle in aqueous solution, ROESY experiments have been performed.[24] The two different situations observed in potentiometry are illustrated by the ROESY NMR spectra of the ligands L^4 and L^1 acquired at pD 7.41 where the bicycle is mono- (L^4) or diprotonated (L^1), and for which the spectra are the best-resolved (Figure 1, see Figure S17 for complete spectra). As the ligands display C_S symmetry, protons H2 and H4, and H6 and H8, respectively, are equivalent (see Figure 1 for proton numbering). We followed the correlations involving the H2, the equatorial (eq) and axial (ax) H6, as well as H9, H10 and H11 hydrogen atoms. The dipolar coupling observed between the hydrogens H6 in the axial position and H9 suggests that the piperidine ring involving N7 is in chair conformation for both ligands.

In order to assess the conformation of the N3 piperidine ring, the relative position of H2 with respect to H6ax/eq protons, and consequently their dipolar coupling are particularly important. For L^4, the weak correlation observed between H2 and the axial protons H6ax and more importantly the absence of correlation between the H2 and the equatorial H6eq atoms let us deduce that the H2 hydrogen atoms are in axial position. This confirms the chair-chair conformation of the monoprotonated HL^4 (with both pyridines in *cis* position), and the hydroxyl group pointing towards the nitrogen N3. For the diprotonated H_2L^1, the

correlation between H2 and H6ax is present, but we also observe a stronger correlation (ROE twice as intense) of H2 with the equatorial H6 protons. This, as well as the high intensity ROE signal between H2 and H11 point to a boat conformation for the N3 piperidine, thus a boat-chair conformation for H_2L^1. In a similar way, the analysis of the ROESY spectra allowed us to conclude a chair-chair and boat-chair conformation for HL^2 and H_2L^3, respectively (Figure S17).

These NMR results are in perfect agreement with the conclusions of the potentiometric titrations and indicate that the mono-protonated bispidines (HL^2 and HL^4) adopt a chair-chair conformation, with a "bicyclic cage" available for metal complexation. In contrast, bispidines which undergo double protonation on the bicycle (H_2L^1 and H_2L^3) have a boat-chair conformation without the characteristic bicyclic bispidine cavity.

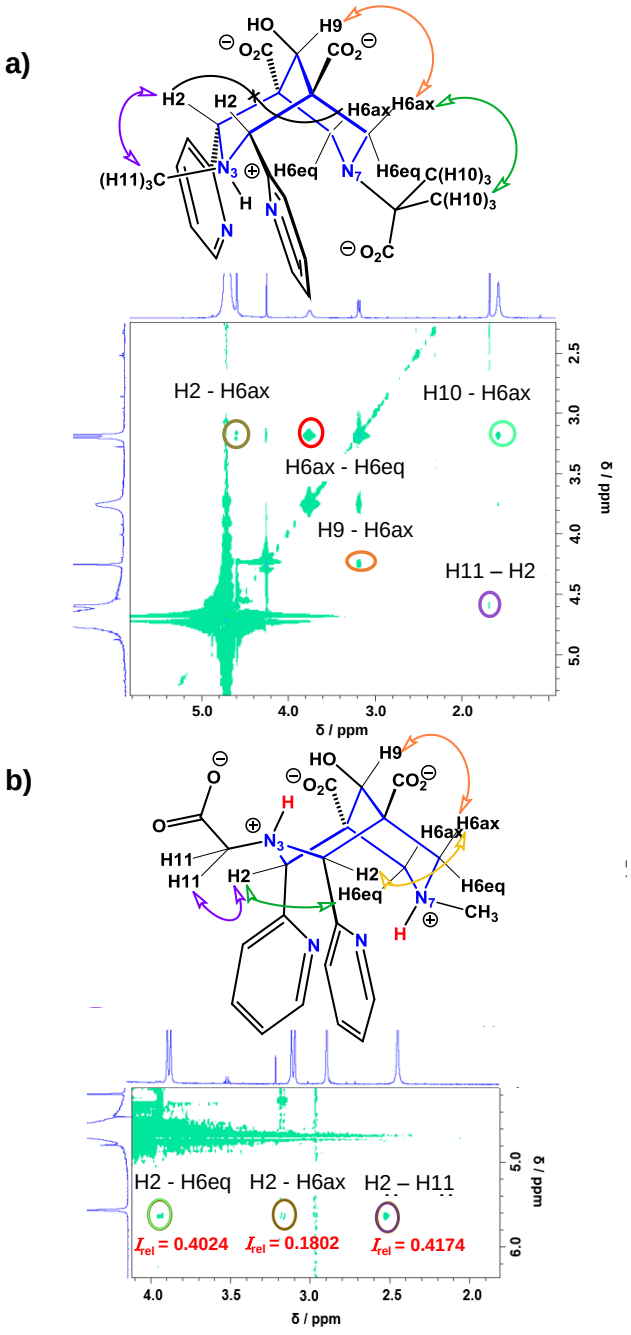

Figure 1. ROESY spectra of HL^4 (a) and H_2L^1 (b). pD 7.41 and c_L = 3.5 mM. 600 MHz.

Relationship between ligand conformation and the physico-chemical properties of the complexes

Formation and thermodynamic stability of MnL complexes

The formation of the Mn^{2+} chelates was followed as a function of time by measuring the water proton longitudinal relaxation times after mixing the metal ion and the ligand at pH 7.36 in buffered solutions (Figure 2). A large difference is observed in the formation rate between the ligands in chair-chair (HL^2[15] and HL^4) and in boat-chair (H_2L^1 and H_2L^3) conformation, clearly indicating the importance of the ligand structure for the kinetics. With H_2L^1 and H_2L^3, complex formation is very fast and complete in less than 2 min. In contrast, for HL^2 and HL^4, the formation is slow (~30 min and 2 h are needed to complete the reaction, respectively). Slow complex formation has been previously reported for other bispidine ligands, all in chair-chair conformation, in this pentadentate family.[14-15]

The slow formation of MnL^2 and MnL^4 complexes likely implies the formation of an intermediate in a rapid equilibrium step where the metal ion has not yet fully entered the bicyclic cage and the bicycle amine remains protonated. The second, rate-determining step involves the deprotonation of the nitrogen, with the subsequent entering of the Mn^{2+} into the coordination cavity. Such an intermediate was identified in the formation of MnBisp3.[16] In order to assess the protonation state of the intermediate, we followed a protocol similar to that previously used to study the formation kinetics of Gd(DOTA).[25] We have monitored the pH change in a slightly buffered solution (25 mM HEPES) after mixing equivalent amounts of Mn^{2+} and L^4 at pH 7.36, where the ligand is monoprotonated. We observe a slow pH drop over time (Figure 2.d), occurring on the same time-scale as the changes in the relaxometric monitoring (Figure 2c). The amount of H^+ ions liberated in this process can be also determined by titrating the same amount of buffer with an HCl solution from the starting to the final pH. This amount corresponds to one equivalent of proton, indicating that the intermediate is the $MnHL^4$ complex.

The slower complexation with HL^2 with respect to HL^4 is due to the presence of the methyl groups in α position of the acetate. The same phenomenon was reported for lanthanide DOTMA chelates which have 3 orders of magnitude slower formation than the analogue DOTA complexes ($DOTMA^{4-}$ = (1R,4R,7R,10R)-α,α',α'', α'''-tetramethyl-1,4,7,10-tetraazacyclododecane-1,4,7,10-tetraacetate; $DOTA^{4-}$ = 1,4,7,10 –tetraazacyclodecane-1,4,7,10-tetraacetate).[19a]

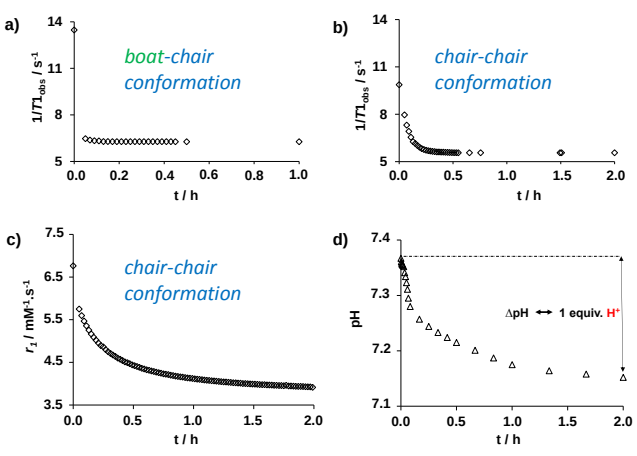

Figure 2. a-c) Variation of the longitudinal relaxation rates as a function of time after mixing equivalent amounts of Mn^{2+} and $H_2\mathbf{L^1}$ (a), $H\mathbf{L^2}$ (b) and $H\mathbf{L^4}$ (c) respectively; pH 7.36, 25 °C, $c_{Mn2+} = c_L$ = 1.5 mM for Mn/$H\mathbf{L^2}$ and Mn/$H\mathbf{L^4}$, and 1.65 mM for Mn/$H_2\mathbf{L^1}$, c_{HEPES} = 50 mM, 60 MHz. d) Variation of pH as a function of time after mixing Mn^{2+} and $H\mathbf{L^4}$; $c_{\mathbf{L4}} = c_{Mn2+}$= 2.5 mM, c_{HEPES} = 25 mM. I = 0.1 M NaCl.

Because of the slow formation of the Mn^{2+} complexes with L^2 and L^4, their stability constants were determined by potentiometry in batch samples between pH 2 and 7; while for L^1 and L^3 direct titrations were performed, as well as for all Zn-L systems (Figure S18). The stability constants determined for the MnL and ZnL complexes (Table 2) reveal some unexpected trends. First of all, there is a high protonation constant for all four MnL^1, ZnL^1, MnL^3 and ZnL^3 complexes in the basic region, indicating that one of the bicycle amines remains protonated in the complex. This protonated amine cannot be involved in metal coordination, suggesting that the ligand retains the boat-chair conformation at least in the protonated complex. This is also in accordance with the fast formation of the complexes which does not require the deprotonation of the amine. We should stress that the comparison of the ligand titration curves in the absence and in the presence of the metal ions (with one equivalent proton between the inflection points of the two curves) unambiguously indicates that the deprotonation step observed for the complexes at pH~9 is not related to potential hydrolysis of the metal ions, but to the deprotonation of the ligand (Figure S18). In addition, L^1 and L^3 form more stable complexes than L^2 and L^4, which confirms a different coordination sphere. The difference is particularly striking for Zn^{2+}, with 3-5 orders of magnitude higher K_{ZnL} stability constants for the L^1 and L^3 analogues (though the conditional stabilities expressed via the pM values are closer). Finally, L^3 forms a slightly more stable Mn^{2+} complex than L^1 (pMn = 8.48 vs. 6.47), which may be ascribed to the coordination of the second carboxylate group at N7.

The boat-chair conformation for $ZnHL^1$ was indeed confirmed via the characteristic correlations in ROESY NMR experiments (Figure S19). We note that, in contrast to the non-complexed ligand, the ROE intensity is no longer similar for the H2/4-H6/8eq and H2/4-H11 correlations, but the latter is far more intense. This is probably due to a conformation change upon complexation with Zn^{2+}, associated to the involvement of the donor groups around H11 and H2/4 protons in Zn^{2+} coordination. In order to get further insight into the structure of the Zn^{2+} complex, DFT calculations have been performed at the PBE0/def2-SVP level. A series of different coordination geometries have been modeled for [$ZnHL^1$] and the mono-hydrated analogue [$ZnHL^1(H_2O)$] and their relative energies have been compared (Figure S20 and Table S1). The optimized structure suggests that [$ZnHL^1(H_2O)$] (Figure 3) is the most stable and that the boat-chair conformation of the ligand is retained leading to a pentadentate coordination of Zn^{2+} by N7, the two pyridyl nitrogens, the carboxylate and a water molecule with a square pyramidal geometry. Such coordination geometry is not unusual for Zn^{2+} complexes with bispidine-type ligands.[26] In addition, the boat-chair conformation is in agreement with the correlations observed by NMR ROESY experiments with distances of 2.17 Å for H2-Hd, 2.50 Å for H2-H11, 2.45 Å for H9-H6ax and 2.39 Å and 2.41 Å for CH_3-H6eq and CH_3-H6ax, respectively. No correlation is seen between CH_3 and H9 (d = 4.24 Å) whereas it should be expected in the case of a chair-boat conformation (d = 1.9 Å).

The paramagnetic Mn^{2+} analogue is not amenable to an NMR study, but on the basis of DFT calculations (Table S1 and Figure S21), we hypothesized that [$MnHL^1$(H2O)] is also the most stable species and displays a ligand in boat-chair conformation and a similar square pyramidal coordination sphere. In addition, metal coordination of the pyridine functions is supported by UV-Vis spectra which show an intensity increase of the pyridine absorbance upon Mn^{2+} complexation of HL^1, in a similar manner to what is observed for L^4 where we know that the pyridines are involved in complexation (Figure S22). Unfortunately, all attempts to crystallize the complexes for X-ray analysis were unsuccessful.

In overall, the stability of the Mn^{2+} complexes is modest (Table 2), as compared to the best Mn^{2+} chelating ligands described in the literature in the context of MRI. The pMn values are considerably lower than that of Mn(PC2A-EA) for instance (pMn = 9.27).[10b] For all cases, the stability of Zn^{2+} complexes is higher compared to their Mn^{2+} analogues, obeying the Irving-Williams rule.[27] The species distribution curves calculated for 1 mM MnL concentration by using the stability and protonation constants in Table 2 are represented in Figures 4 and S23. The comparison of the distribution curves for the Mn-L^1 and Mn-L^4 systems (Figure 4) illustrates well the difference between the two conformations: at physiological pH, the $MnHL^1$ complex in boat-chair conformation is exclusively mono-protonated, in contrast to the fully deprotonated form for the chair-chair conformation MnL^4. The distribution curves are nicely corroborated with the pH-dependent relaxivities measured in aqueous solution of the Mn^{2+} complexes; in particular, the progressive relaxivity decrease between pH 2-4 follows the decreasing concentration of free Mn^{2+} upon complex formation.

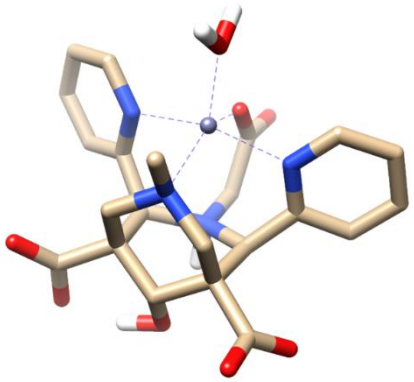

Figure 3. DFT structure of the [$ZnHL^1(H_2O)$] complex.

Table 2. Stability constants of ML complexes. I = 0.15 M NaCl; 298 K. Values in parenthesis correspond to one standard deviation.

	L^1	$L^{2\,a}$	L^3	L^4	PC2A-EA[b]
$\log K_{MnL}$	12.81(5)	11.26	14.17(3)	11.60(4)	19.01
$\log K_{MnHL}$	9.54(3)	3.20	9.15(2)	4.52(3)	6.88
$\log K_{MnH2L}$	3.70(4)	-	3.73(1)	-	2.50
$\log K_{MnH3L}$	-	-	2.20(1)	-	-

logK_{ZnL}	18.49(3)	13.72	17.45(4)	14.90(4)	-
logK_{ZnH}	9.35(2)	3.26	8.94(3)	3.43(2)	-
logK_{ZnH2L}	3.44(2)	-	3.44(3)	-	-
logK_{ZnH2L}	-	-	2.26(4)	-	-
pMn[c]	6.47	7.06	8.48	6.63	9.27
pZn[c]	9.21	8.29	9.98	8.28	-

[a] ref. [15]; [b] ref. [10b]; [c] $c_M = c_L = 10^{-5}$ M ; pH 7.4

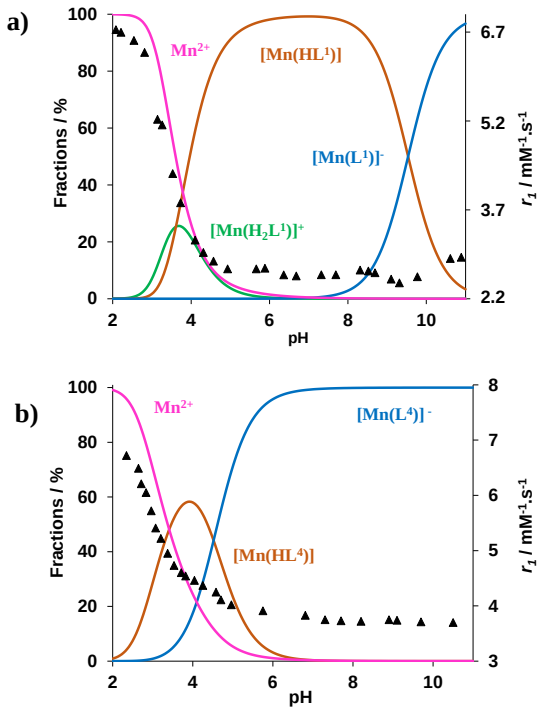

Figure 4. Species distribution curves calculated for Mn-**L**[1] (a) and Mn-**L**[4] (b) and pH-dependent relaxivities (▲) measured at 25 °C, 60 MHz. I = 0.15 M NaCl.

Kinetic inertness

The kinetic inertness of the Mn^{2+} chelates has been evaluated via transmetallation reactions in the presence of 50 equiv. of Zn^{2+} at different pH values, at 37 °C (Figure S24). For a direct illustration of the different dissociation kinetics between the four systems, we present the evolution of the relaxivity as a function of time at pH 6 (Figure 5). Again, there is a clear-cut difference between the two different conformations. The dissociation half-life is 1.48 h for $MnHL^1$ and 3.85 h for $MnHL^3$, in contrast to MnL^2 and MnL^4 for which even after 120 days the dissociation is limited to ~46 % and 23 %, respectively. Since at pH 6 the conversion is very small for MnL^2 and MnL^4, we rather compare the observed dissociation rate constants (k_{obs}) and half-lives at pH 4 for the four complexes (Table 3). The 3-4 orders of magnitude slower dissociation for MnL^2 and MnL^4 in chair-chair conformation evidences the primordial role of this conformation for the kinetic inertness of bispidine complexes. The dissociation half-life doubles for MnL^4 vs. MnL^2 which shows that the methyl groups introduced in α position on the N7 acetate reinforce the kinetic inertness, thanks to the steric hindrance induced. Similar conclusion was previously found for macrocyclic lanthanide complexes.[19b]

In the case of $MnHL^1$ and $MnHL^3$, we also studied the dissociation at different Zn^{2+} concentrations between pH 3.1 and 6.0 (Figure 6). For MnL^2 and analogue complexes, we have previously shown that the dissociation rates have negligible dependence on the concentration of the exchanging metal.[14-15] In contrast, for $MnHL^1$ and $MnHL^3$, k_{obs} increases with increasing acidity and with decreasing Zn^{2+} concentration. This latter finding indicates the formation of a catalytically inactive dinuclear MnLZn intermediate, usually referred to as a «dead-end» complex, observed for other systems as well.[28]

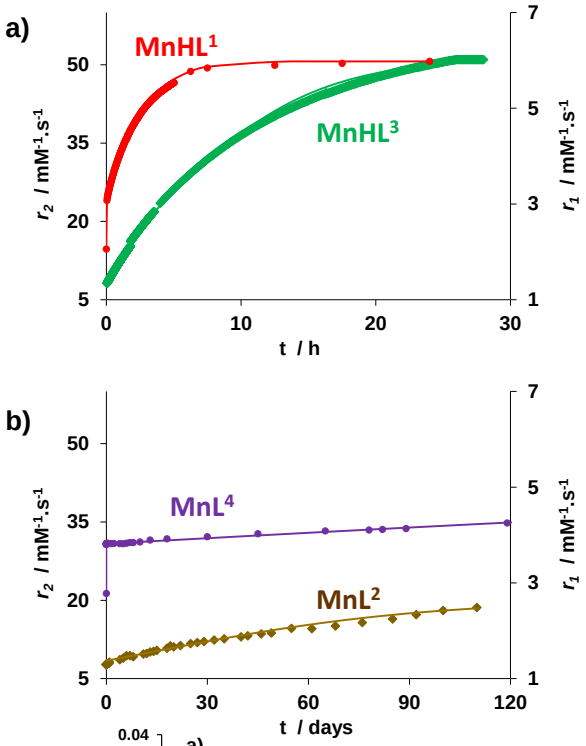

Figure 5. Dissociation of the complexes in the presence of 50 eq. of Zn^{2+}, pH 6, 37°C. Variation of the longitudinal r_1 (MnHL[1] (a) and MnL[2] (b)) and transverse r_2 (MnHL[3] (a) and MnL[4] (b)) relaxivities as a function of time.

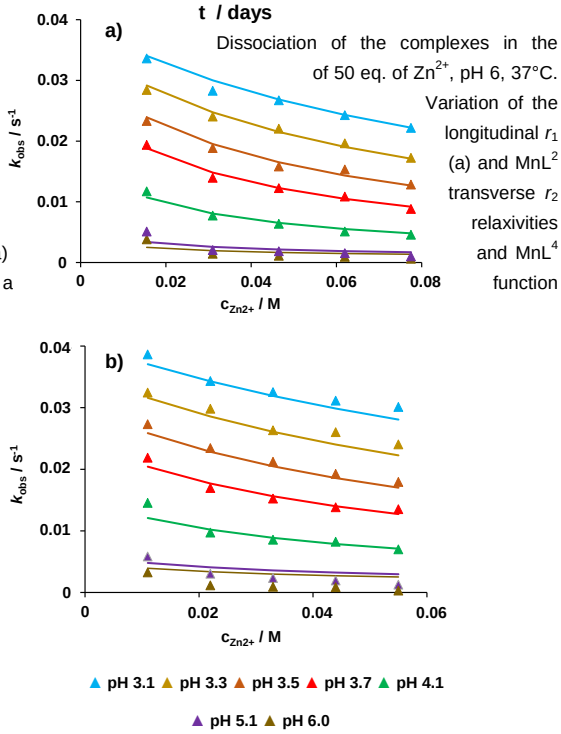

Figure 6. Observed dissociation rate constants as a function of the Zn^{2+} concentration at different pH values for $MnHL^1$ (a) and $MnHL^3$ (b). The lines correspond to the fit to the experimental points as described in the text.

For both $MnHL^1$ and $MnHL^3$, only protonated complexes exist in the pH range investigated. By taking into account the proton- and the metal-assisted pathways and the presence of the differently protonated species, the overall dissociation can be illustrated as shown on Scheme 3.

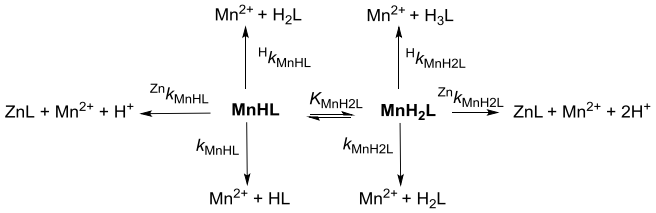

Scheme 3. Dissociation pathways considered for $MnHL^1$ and $MnHL^3$.

By considering all dissociation pathways in Scheme 3, Equation 1 can be derived for the reaction rate:

$$-\frac{d[MnL]_{tot}}{dt} = k_{obs}[\mathrm{MnL}]_{tot}$$

$$-\frac{d[MnL]_{tot}}{dt} = k_{MnHL}[\mathrm{MnHL}] + {}^{H}k_{MnHL}[\mathrm{MnHL}][H^+] + {}^{Zn}k_{MnHL}[\mathrm{MnHL}][Zn^{2+}] + k_{MnH2L}[\mathrm{MnH_2L}] + {}^{Zn}k_{MnH2L}[\mathrm{MnH_2L}][Zn^{2+}] + {}^{H}k_{MnH2L}[\mathrm{MnH_2L}][H^+] \quad (1)$$

In Equation 1, each term represents a dissociation pathway. As the overall MnL concentration is the sum of the concentrations of the differently protonated species, Equation 2 can be derived for the pseudo-first-order rate constant, k_{obs}; with $k_0 = k_{MnHL}$, $k_1 = {}^{H}k_{MnHL}\cdot K_{MnH2L}$, $k_2 = {}^{H}k_{MnH2L}\cdot K_{MnH2L}\cdot K_{MnH3L}$, $k_3 = {}^{Zn}k_{MnHL}\cdot K_{MnLZn}$, $k_4 = {}^{Zn}k_{MnH2L}\cdot K_{MnH2L}$, $k_5 = {}^{H}k_{MnH2L}\cdot K_{MnH2L}\cdot K_{MnH3L}$ and $k_6 = {}^{Zn}k_{MnH2L}\cdot K_{MnH2L}\cdot K_{MnH3L}$.

$$k_{obs} = \frac{k_0 + k_1[H^+] + k_2[H^+]^2 + k_3[Zn^{2+}] + k_4[H^+][Zn^{2+}]}{1 + K_{MnH2L}[H^+] + K_{MnH2L}K_{MnH3L}[H^+]^2 + K_{MnLZn}[Zn^{2+}]} \quad (2)$$

The experimental k_{obs} data in Figure 6 were fitted to Equation 2 where k_0, k_1, k_2 and k_3 are the rate constants corresponding to the dissociation of the monoprotonated MnHL complex via spontaneous, proton-assisted and metal-assisted mechanisms, respectively, and k_4 characterizes the zinc-catalyzed dissociation of the diprotonated complex. The protonation constants were determined previously by potentiometry and K_{MnLZn} corresponds to the stability constant of the dinuclear complex which forms transitionally during the reaction. For MnL^3, a very small amount of triprotonated complex also exists at the lowest pH of the transmetallation experiments, but due to its very low molar fraction, its contribution to the dissociation could not be evaluated. Indeed, the fit indicates that even the terms related to k_0, k_2, k_3 and k_4 are negligible in Eq. (2); if not fixed to zero, the fit yields negative values for k_2 and k_4, and the errors are also very high for k_0 and k_3 (Table 3). In overall, this implies that the proton-assisted dissociation of the monoprotonated complex is the only significant pathway under our experimental conditions. The k_1 values characterizing this pathway are 4 orders of magnitude higher than that calculated for the proton-assisted dissociation of MnL^2.[15] We cannot exclude that at higher pH, the spontaneous dissociation of the monoprotonated complexes $MnHL^1$ and $MnHL^3$ also becomes important, and we can speculate that an intramolecular proton transfer from the tertiary amine to a coordinating donor group might occur and yield dissociation.

These kinetic experiments clearly indicate the formation of a dinuclear MnLZn intermediate for $MnHL^1$, $MnHL^3$, while it was not observed for MnL^2 or other Mn^{2+} bispidine chelates in chair-chair conformation.[14-15] We should note that it is impossible to assess from these experiments if this dinuclear complex remains protonated or not.

While $MnHL^1$ and $MnHL^3$ dissociate several orders of magnitude faster than MnL^2, MnL^4 or other previously investigated bispidine analogues, their kinetic inertness remains reasonably good ($t_{1/2}$ of few hours at pH 6, 50 eq. of Zn^{2+}, 37°C, Table 3) in comparison to Mn^{2+} complexes currently investigated as potential MRI agents, like MnPyC3A ($t_{1/2}$ = 0.29 h at pH 6, 25 eq. Zn^{2+}, 37 °C),[9b] though it is lower than that for Mn(PC2A-EA), one of the most inert non-bispidine complexes ($t_{1/2}$ = 54.4 h, under similar conditions).[10b] In overall, these studies demonstrate the versatility of bispidine ligands, as well as the primordial role of the chair-chair conformation and thus the bicyclic coordination cavity of the ligand for the design of highly inert Mn^{2+} chelates.

Table 3. Half-lives ($t_{1/2}$) and rate constants characterizing the dissociation of Mn^{2+} complexes (37 °C, I = 0.1 M NaCl).

	MnH**L**[1]	Mn**L**[2] [b]	MnH**L**[3]	Mn**L**[4]	MnPC2 A-EA[10b]
$t_{1/2}$ (pH 6)[a]	1.48 h	>120 days	3.85 h	>120 days	54.4 h
$t_{1/2}$ (pH 4) [a]	2.5 min	4.5 days	1.6 min	9.3 days	-
k_0 / s^{-1}	4(9)×10^{-3}	-	4(5)×10^{-3}	-	-
k_1 / $s^{-1}.M^{-1}$	241(8)	1.79×10^{-2} [d]	184(3)	-	0.6 [d]
k_3 / $s^{-1}.M^{-1}$	0.04(3)		0.03(5)		-
K_{MnH2L}	5012 [c]	-	3311 [c]	-	102 [e]
K_{MnLZn}	51(4)	-	30(5)	-	

[a] 50 equ. Zn^{2+}, 37 °C

[b] ref. [15]

[c] determined by potentiometry

[d] refers to the proton-assisted dissociation of the non-protonated complex

[e] K_{MnHL}

Relaxation properties and metal coordination mode

The relaxation efficacy of paramagnetic complexes is typically expressed by the relaxivity (r_1) which is the enhancement of the longitudinal water proton relaxation rate in the presence of 1 mM concentration of the agent. Proton relaxivities have been measured for MnHL[1], MnHL[3] and MnL[4] at 25 °C and 37 °C in water (pH 7) in the 0.01-80 MHz proton Larmor frequency range (Figure 7). The relaxivities are considerably lower for the Mn^{2+} chelates in boat-chair conformation: r_1 = 2.59 $mM^{-1}s^{-1}$ and r_1 = 2.79 $mM^{-1}s^{-1}$ for MnHL[1] and MnHL[3], respectively to be compared with r_1 = 3.64 $mM^{-1}s^{-1}$ for MnL[2] [15] and r_1 = 3.71 $mM^{-1}s^{-1}$ for MnL[4] (25 °C, 60 MHz). The reason for these lower relaxivities is the lower hydration number, as it was evidenced by the variable temperature ^{17}O transverse relaxation rates ($1/T_2$). Based on the method proposed by Gale et al.,[29] the hydration number is estimated to q = 0.6 for MnHL[1] (Figure 7), pointing to a hydration equilibrium between mono-hydrated and non-hydrated species. The mono-hydrated species is in agreement with the structure suggested from DFT calculation (Figure S20). The non-hydrated species could be obtained by deprotonation at N7 or coordination of carboxylate groups. A similar result is to be expected for MnHL[3], although the lack of a maximum in the $1/T_2$ vs. temperature curve (Figure 7) prevents the application of Gale's approach. Nevertheless, the close-to-zero ^{17}O transverse relaxation rates above 290 K are indicative of a non-hydrated complex at these temperatures. The lower hydration number of MnHL[1] and MnHL[3] is also coherent with the relatively high stability of these complexes in boat-chair conformation.

As a comparison, we calculate q = 0.8 for MnL[4] (Figure S25), while q = 1.0 was found previously for MnL[2].[15] With a hydration equilibrium, the proper analysis of the NMRD curves becomes too complex (the molar fraction of two species changes with temperature), hence no data adjustment was done for MnHL[1] and MnHL[3] complexes.

In the case of MnL[4], we have analyzed the ^{17}O NMR transverse relaxation rates and the proton relaxivities according to the usual Solomon-Bloembergen-Morgan theory of paramagnetic relaxation. As for previous analogous systems,[14-15] we have also included a second-sphere contribution to proton relaxivity, which is generated by the non-coordinating carboxylates on the bispidine skeleton. The parameters characterizing water exchange and rotational dynamics obtained from this fit are shown in Table 4, the full list of parameters is given in the Supporting Information. These data indicate great similarity between MnL[4] and MnL[2], as it can be expected. Apart from the water exchange rate (k_{ex}^{298}) which is slightly higher for MnL[4], the activation enthalpy ($\Delta H^{\neq}$) and entropy ($\Delta S^{\neq}$) of the exchange, as well as the rotational correlation time (τ_{rH}^{298}) and its activation energy (E_{rH}) all have practically identical values for the two complexes.

Table 4. Parameters obtained from the fit of ^{17}O NMR and NMRD data.

	MnL[4]	MnL[2] [a]	MnBisp1[b]
q	1	1	1
r_1 /$mM^{-1}s^{-1}$ [b]	3.71	3.64	4.28
k_{ex}^{298} /10^7 s^{-1}	7.7(1)	5.5	5.1
$\Delta H^{\neq}$ / kJ.mol^{-1}	12.7(7)	14.9	10.6
$\Delta S^{\neq}$ / kJ.mol^{-1}	-51(3)	-47	-62
E_{rH} / kJ.mol^{-1}	26(1)	20	22
τ_{rH}^{298} / ps	64(4)[d]	65[d]	72[d]

[a] ref. [15]

[b] ref.[14]

[c] 20 MHz and 25 °C

[d] considering a 2nd sphere relaxivity contribution.

Conclusion

Depending on the nature of the substituents on the bicycle amines, bispidine ligands can have different conformations, with important consequences on their complexation features. We have investigated a series of carboxylate bispidine ligands and demonstrated that the substituent on N3 amine nitrogen has a pivotal role. Potentiometric and ROESY NMR studies have shown that at neutral pH, the methyl derivatives L[2] and L[4] are monoprotonated and have chair-chair conformation, in contrast to the ligands L[1] and L[3] which are protonated on both bispidine amine functions and hence adopt a boat-chair conformation. The different conformations are retained in their Zn^{2+} and Mn^{2+} complexes, and result in drastically different physico-chemical properties. Complex formation and complex dissociation are both several orders of magnitude slower for the Mn^{2+} chelates in chair-chair conformation. The thermodynamic stability of the complexes is also strongly impacted. At pH 7, the Zn^{2+} and Mn^{2+} complexes of L[1] and L[3] in boat-chair conformation are monoprotonated on the bicyclic amine, implying that this nitrogen is not involved in the metal coordination. The hydration number and consequently the relaxation properties of the Mn^{2+} chelates are also affected by ligand conformation. The MnHL[1] and MnHL[3] chelates in boat-chair conformation have less than one inner sphere water molecule, as evidenced by ^{17}O NMR data, and thus reduced relaxivities. In overall, these results

unambiguously prove the importance of bispidine conformation on the physical chemical properties of the complexes, and that the chair-chair conformation is a prerequisite to attain the impressive kinetic inertness exhibited by several examples in this family of Mn^{2+} bispidines.

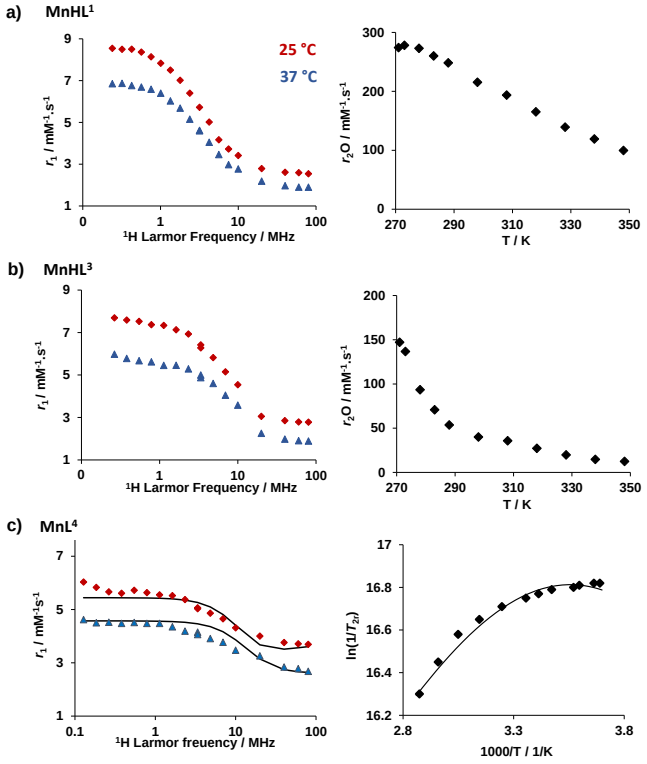

Figure 7. NMRD profiles (left; 25 °C and 37 °C) and temperature-dependent transverse ^{17}O relaxation rates (right, B = 9.4 T) of $MnHL^1$ (a), $MnHL^3$ (b) and MnL^4 (c). For MnL^4, the lines represent the simultaneous fit of ^{17}O NMR and NMRD data to the Solomon-Bloembergen-Morgan theory.

Experimental Section

General procedures. Solvents and starting materials were purchased from Aldrich, Acros and Alfa Aesar and used without further purification, unless stated otherwise. Solvents for high-performance liquid chromatography (HPLC) were HPLC-grade. All aqueous solutions were prepared with Milli-Q water (ρ < 18MΩ). $MnCl_2.4H_2O$ was obtained from Carlo Erba. Chromium powder 99 %, 100 mesh metal basis density = 2.0-3.0g/cm², was obtained from Alfa-Aesar. Intermediates **2_H**, **3, 8** and ligand **H_3L^2** were obtained according to the procedures described previously.[15, 20]

IR spectra were recorded on a Perkin Elmer Spectrum One Spectrophotometer as solid samples and only the most significant absorption bands are given in cm^{-1}. ^1H and ^{13}C NMR spectra and 2D COSY, NOESY, HSQC, and HMBC experiments were recorded either on Bruker Avance 400 and Avance 500 spectrometers (in Strasbourg) or on a Bruker Advance III HD Spectrometer using a 5 mm BBFO probe (in Orléans). ^{13}C NMR spectra were measured with ^1H decoupling. All chemical shifts (δ) values are given in parts per million and are referenced to the solvent.[30] Elemental analyses and mass spectrometry analysis were carried out by the Service Commun d'Analyses of the University of Strasbourg.

Synthesis

Synthesis of H_3L^1.

Compound 5. Potassium carbonate (88 mg, 0.64 mmol, 1.2 equiv.) was dissolved in a solution of **2_H** (300 mg, 0.53 mmol, 1 equiv.) in 30 mL of anhydrous acetonitrile under argon. Then ethyl bromoacetate (71 µL, 0.64 mmol, 1.2 equiv.) was added and the mixture was heated at 80 °C for 16 hours. At the end, K_2CO_3 was filtered and solvent was removed under vacuum. The product was used for the next step without purification.

^1H NMR ($CDCl_3$, 400 MHz) : δ (1.13 (t, ^3J = 7.2 Hz, 3H, H19); 2.57 (s, 2H, H11); 3.51 (s, 6H, H16); 3.74 (s, 3H, H14/15); 3.88 (s, 3H, H14/15); 4.02 (q, ^3J = 7.2 Hz, 2H, H18); 4.28 (m, 4H, H6 + H8); 4.64 (s, 2H, H10); 4.98 (s, 1H, H9); 5.59 (s, 2H, H2 + H4); 6.53 (dd, ^3J = 8.4 Hz, ^4J = 2.4 Hz, 1H, H12); 6.60 (d, ^4J = 2.4 Hz, 1H, H13); 7.20 (m, 2H, Hb); 7.30 (d, ^3J = 8.1 Hz, 2H, Hd); 7.55 (d, ^3J = 8.4 Hz, 1H, H11); 7.61 (td, ^3J = 7.9 Hz, ^4J = 1.7 Hz, 2H, Hc); 8.27 (m, 2H, Ha).

Mass Spectrometry: (ESI^+/MS): *m/z* = 649.28 $[M + H]^+$, calculated for $C_{34}H_{41}N_4O_9$: 649.28.

Compound 6. The crude product of **5** (0.44 mmol) was dissolved in a mixture of TFA (5 mL) and DCM (10 mL) and the solution was heated for 16 hours at reflux. At the end the solvent was removed under vacuum. Then, the crude product was dissolved in MeOH and heated under vacuum. A white precipitate was obtained. The precipitate was filtered and the solvent was removed under vacuum. The crude product was finally purified by FPLC (SiO_2, DCM/MeOH) to give **6**.2TFA (135 mg) with a 42 % yield.

^1H NMR ($CDCl_3$, 400 MHz): δ 1.09 (t, ^3J = 7.1 Hz, 3H, H13); 2.62 (s, 2H, H11); 3.49 (m, 8H, H10 + $H6/8_{ax}$); 3.98 (q, ^3J = 7.1 Hz, 2H, H12); 4.31 (m, 2H, $H6/8_{eq}$); 4.57 (s, 1H, H9); 5.59 (s, 2H, H2/4); 7.26 (m, 2H, Hb); 7.32 (m, 2H, Hd); 7.64 (t, ^3J = 7.3 Hz, 2H, Hc); 8.68 (m, 2H, Ha).

^{13}C NMR ($CDCl_3$, 126 MHz): δ 14.15; 46.48; 49.12; 49.97; 52.85; 60.45; 62.28; 72.54; 123.87; 126.39; 137.00; 150.21; 156.09; 169.53; 170.20.

Mass Spectrometry: (ESI^+/MS): *m/z* = 499.21$[M + H]^+$, calculated for $C_{25}H_{31}N_4O_7$: 499.21.

Elemental Analysis: Calculated for $C_{25}H_{30}N_4O_7.2(CF_3COOH)$, C, 47.94, H, 4.44, N, 7.71. Found: C,47.61, H, 4.5, N, 7.49.

H_3L^1. Potassium carbonate (131 mg, 0.95 mmol, 1.2 equiv.) was dissolved in a solution of **6** (390 mg, 0.79 mmol, 1 equiv.) in 40 mL of anhydrous acetonitrile under argon. Then iodomethane (59 µL, 0.95 mmol, 1.2 equiv.) was added and the mixture was heated at 80 °C for 16 hours. Subsequently, K_2CO_3 was filtered and the solvent was removed under vacuum. The crude product was then used for the next step without purification and dissolved in a mixture of H_2O (30 mL) and THF (20 mL). Lithium hydroxide (128 mg, 5.35 mmol, 5 equiv.) was added. The solution was stirred for 16 hours at room temperature. At the end of the reaction, the solvent was evaporated, the crude product was dissolved in a minimum of water and the pH was adjusted to 2 with diluted HCl_{aq} solution. The solution was then purified by FPLC (C_{18}, 97/3 H_2O/MeOH to 50/50 H_2O/MeOH) to give **H_3L^1**.HCl.0.5.H_2O (160 mg) with a 41 % yield.

^1H NMR (MeOD, 400 MHz): δ 2.62 (s, 2H, H11), 3.04 (s, 3H, H10); 3.39 (d, 2H, H6/8ax, $^4J_{H6axH8ax}$ = 12.7 Hz); 4.21 (d, 2H, H6/8eq, $^4J_{H6eqH8eq}$ = 12.7 Hz); 4.41 (s, 1H, H9); 5.73 (s, 2H, H2/H4); 7.35 (m, 2H, Hb); 7.46 (d, ^3J = 7.7 Hz, 2H, Hd); 7.76 (m, 2H, Hc); 8.69 (m, 2H, Ha).

^{13}C NMR (MeOD, 126 MHz): δ 41.88; 49.55; 49.65; 57.56, 62.60; 72.86; 123.40; 127.07; 137.02; 149.32; 157.28; 171.57; 172.39.

Elemental Analysis: Calculated for $C_{22}H_{24}N_4O_7HCl.0.5H_2O$ C, 52.65, H, 5.22, N, 11.16. Found: C,52.80, H, 5.32, N, 11.61.

Mass Spectrometry: (ESI^-/MS): *m/z* = 455.15 $[M - H]^-$, calculated for $C_{22}H_{23}N_4O_7$: 455.15.

Synthesis of H_4L^3. Potassium carbonate (212 mg, 1.53 mmol, 2.4 equiv.) was dissolved in a solution of **8** (263 mg, 0.64 mmol, 1 equiv.) in 50 mL of anhydrous acetonitrile under argon. Then, ethyl bromoacetate (182 µL, 1.6 mmol, 2.5 equiv.) was added and the mixture was heated at 80 °C for 16 hours. At the end, K_2CO_3 was filtered and the solvent wwas removed under vacuum. The product is used for the next step without purification. The crude product was dissolved in a mixture of H_2O (10 mL) and THF (5 mL) and lithium hydroxide (123 mg, 5.12 mmol, 8 equiv.) was added. The solution was stirred for 16 hours at room temperature. At the end, the solvent was evaporated and the crude product was purified by FPLC (C_{18}, 97/3 H_2O/MeOH to 50/50 H_2O/MeOH) to give **H_4L^3**. 2 LiOH.H_2O (150 mg) with a 41 % yield.

^{1}H NMR (CD_3OD, 400 MHz): *δ* 2.82 (s, 2H, H10/H11); 3.60 (m, 2H, H6/8ax); 3.75 (m, 2H, H6/8eq); 3.75 (s, 2H, H10/H11); 4.42 (s, 1H, H9); 5.75 (s, 2H, H2/H4); 7.36 (m, 2H, Hb); 7.66 (m, 2H, Hd); 7.80 (m, 2H, Hc); 8.68 (m, 2H, Ha).

^{13}C NMR (D_2O, 150 MHz): *δ* 50.83; 56.22; 59.10; 63.89; 72.82; 124.66; 127.23; 140.46; 146.69; 155.27; 170.95; 174.73; 176.59.

Mass Spectrometry: (ESI^-/MS): *m/z* = 499.14 $[M - H]^-$; 505.15 $[M – 2H + Li]^-$, calculated for $C_{23}H_{23}N_4O_9$: 499.15

Elemental Analysis: Calculated for $C_{23}H_{24}N_4O_9.2(LiOH).H_2O$, C, 48.78, H 4.98, N, 9.89. Found: C,48.78, H, 5.02, N, 10.16.

Synthesis of H_3L^4. Potassium carbonate (106.4 mg, 0.77 mmol, 1.1 equiv.) was dissolved in a solution of **3** (300 mg, 0.70 mmol, 1 equiv.) in 30 mL of anhydrous acetonitrile under argon. Then methyl 2-bromo-2-methylpropionoate (100 µL, 0.77 mmol, 1.1 equiv) was added and the mixture was heated at 80 °C for 16 hours. At the end, K_2CO_3 was filtered and solvent was removed under vacuum. The product was used for the next step without purification. The crude product was dissolved in a mixture of H_2O (20 mL) and THF (10 mL) and lithium hydroxide (83.82 mg, 3.5 mmol, 5 equiv.) was added. The solution was stirred for 16 hours at room temperature. At the end, the solvent was evaporated and the crude product was dissolved in a minimum of H_2O and the pH was adjusted to 2 with aqueous HCl. The solution was then purified by FPLC (C_{18}, 97/3 H_2O/MeOH to 50/50 H_2O/MeOH) to give **H_3L^4**.2HCl.0.5H_2O (125 mg) with a 31 % yield.

^{1}H NMR (MeOD, 400 MHz): *δ* 1.63 (br s, 6H, H11); 2.12 (br s, 3H, H10); 3.13 (m, 2H, H6/8ax); 3.59 (m, 2H, H6/8eq); 4.37 (br s, 1H, H9); 5.31 (br s, 2H, H2 + H4); 7.47 (m, 2H, Hb); 7.75 (m, 2H, Hd); 7.90 (m, 2H, Hc); 8.72 (m, 2H, Ha).^{13}C NMR (MeOD, 126 MHz): *δ* 44.81; 48.70; 48.85; 51.65; 67.09; 67.51; 73.52; 122.74; 125.82; 136.83; 138.94; 149.16; 159.61; 179.14; 183.28.

Mass Spectrometry: (ESI^+/MS): *m/z* = 485.19 $[M+H]^+$, calculated for $C_{24}H_{29}N_4O_7$: 485.20.

Elemental Analysis: Calculated for $C_{24}H_{28}N_4O_7.2HCl.0.5H_2O$, C, 50.89, H, 5.52, N, 9.89. Found: C, 50.77, H, 5.71, N, 10.33.

^{1}H NMR studies of ZnL^4. The zinc(II) complex with ligand **L^4** was synthesized *in situ* by mixing equimolar amounts of ligand **L^4** and $ZnCl_2$ in D_2O (C ~10^{-2} M, pD = 7). A white precipitate was obtained which was isolated by centrifugation and dissolved in deuterated methanol and characterized by ^{1}H, ^{13}C and ^{1}H-^{1}H COSY NMR. The absence of ligand was confirmed by the NMR spectra.

^{1}H NMR (MeOD, 400 MHz): *δ* 1.13 (s, 6H, H11); 2.08 (s, 3H, H10); 2.39 (d, 2H, H6/8ax, $^4J_{H6axH8ax}$ = 12.8 Hz); 2.61 (d, 2H, H6/8eq, $^4J_{H6eqH8eq}$ = 12.8 Hz); 4.10 (s, 1H, H9); 5.02 (s, 2H, H2 + H4); 7.66 (m, 4H, Hb + Hd); 8.06 (td, J_1 = 7.9 Hz, J_2 = 1.3 Hz, 2H, Hc); 8.74 (m, 2H, Ha).

^{13}C NMR (MeOD, 126 MHz): *δ* 23.15; 46.61; 51.41; 53.23; 53.78; 67.70; 68.74; 75.18; 128.15; 128.94; 143.14; 150.88; 157.83; 178.59; 186.67.

Sample preparation

Ligand concentrations were determined by adding an excess of $ZnCl_2$ solution to the ligand solution and titrating the metal excess with standardised Na_2H_2EDTA in urotropine buffer (pH 5.6 –5.8) in the presence of Xylenol Orange as an indicator. The concentrations of the metal solutions were determined by complexometric titrations with standardised Na_2H_2EDTA.

For kinetic, relaxometric and ^{17}O NMR measurements, the MnL complexes have been prepared by mixing equimolar solutions of $MnCl_2$ and the ligands and adjusting the pH to 7. The pH was checked and readjusted if needed until full complex formation (no more pH drop).

Formation of the MnL complexes, potentiometric and UV-Vis studies

To follow the formation of Mn^{2+} complexes by relaxometry, we mixed the ligand and Mn^{2+} in 1:1 molar ratio ($c_{Mn} = c_L$ = 1.5 mM, c_{HEPES} = 50 mM, I = 0.1 M NaCl) at 25 °C, pH 7. The reactions were monitored by measuring the water proton relaxation rates at 60 MHz on a Bruker Minispec relaxometer.

For potentiometric titrations, carbonate-free 0.1 M NaOH and 0.1 M HCl were prepared by dilution of concentrated solutions from Fisher Chemicals. Potentiometric titrations were performed in 0.15 M aqueous NaCl under nitrogen atmosphere and the temperature was controlled at 25 ± 0.1 °C with a circulating water bath. The p[H] (p[H] = -log[H+], concentration in molarity) was measured in each titration with a combined pH glass electrode (Metrohm) filled with 3 M KCl. A 702 SM titrino system (Metrohm) was used for the titrations. Prior to each experiment, the electrode was calibrated as a hydrogen concentration probe by titrating known amounts of HCl with NaOH in 0.1 M electrolyte solution.[31] A plot of potential versus p[H] allows the determination of the electrode standard potential (E°) and the slope factor (f). The GLEE program was used for the glass electrode calibration.[32] Continuous potentiometric titrations with 0.1 M NaOH were conducted on aqueous solutions containing 1.5-2.0 mM of ligand in 0.15 M NaCl (V_0 = 5 mL), with 2 minutes waiting time between successive points. The titrations of the metal complexes were performed with the same ligand solution to which 1 equivalent of the metal cation had been added. To determine the stability constant of MnL^1 and MnL^3, an automatic titration was carried out, with 5 mins waiting time between successive points. In the case of MnL^4, batch samples (0.5 mL) were prepared between pH = 2.5 and 7.0 at 1:1 Mn:L ratio ($c_{Mn} = c_L$ = 1.5 mM, 0.15 M NaCl). The samples were kept at 25°C until the equilibrium state was reached (1 day at pH = 2.5 and ~2 hours at pH = 6.5). This was verified by monitoring the stabilization of the relaxivity and the pH values in the samples over time. Experimental data were refined using the computer program Hyperquad 2008.[33] All equilibrium constants are concentration quotients rather than activities and are defined as :

$$K_{mlh} = \frac{[M_m L_l H_h]}{[M]^m [L]^l [H]^h}$$

The ionic product of water at 25 °C and 0.15 M ionic strength is pK_w = 13.77.[34] Fixed values were used for pK_w, ligand acidity constants and total concentrations of metal, ligand and acid. All values and errors (one standard deviation) reported are at least the average of two independent experiments.

UV-Vis spectra of HL^1 and L^4 and their Mn^{2+} complexes have been recorded at pH 7.36, c = 0.045 mM, I = 0.1 M NaCl, on a Perkin Elmer Lambda 19 spectrometer at 25 °C.

Dissociation kinetic experiments

Kinetic inertness was assessed at 37°C and in 0.1 M NaCl, via transmetallation studies of MnL complexes (1 mM) with Zn^{2+} at pH = 6 (0.030 M MES buffer), and at pH = 3.1 (0.050 M KH-phthalate buffer), pH = 3.7 and pH = 4.1 (0.03 M dimethyl-piperazine), and pH = 5 (0.030 M N-methylpiperazine), in the presence of 50-fold excess of Zn^{2+} to guarantee pseudo-first order conditions. For the duration of the experiments (up to several months), the samples were stored in a thermostat at 37 °C and the water proton relaxation rates at 60 MHz were monitored over time using a Bruker Minispec relaxometer. The pH was controlled for each sample at the end of the kinetic measurements to confirm that it remained stable during the experiment. The analysis of the experimental data was performed using Visualiseur/Optimiseur running on a MATLAB 8.3.0 (R2014a) platform. Transmetallation reactions were also carried out at different Zn^{2+} concentrations (between 10 and 50 mM) for MnL^1 and MnL^3 complexes to assess Zn^{2+} dependence.

Relaxometric measurements and ^{17}O NMR studies

Proton NMRD profiles of $MnHL^1$ and $MnHL^3$ were recorded in an aqueous solution (1.9 and 1.2 mM, respectively; pH = 7.0) on a Stelar SMARTracer Fast Field Cycling relaxometer (0.01-10 MHz) and a Bruker WP80 NMR electromagnet adapted to variable field measurements (20-80 MHz) and controlled by a SMARTracer PC-NMR console. The temperature was monitored by a VTC91 temperature control unit and maintained by a gas flow. The temperature was determined by previous calibration with a Pt resistance temperature probe.

Variable temperature ^{17}O transverse (T_2) relaxation times of aqueous solution of manganese complexes (for MnL^1: c_{MnL} = 4.14 mol/kg, pH = 7.4; for MnL^3: c_{MnL} = 4.50 mol/kg, pH = 7.0) were measured using a Bruker ARX 400 spectrometer (9.4 T). The absence of free metal ion was checked by the Xylenol Orange test and the concentration of Mn^{2+} was checked by the chemical shift measurement of tert-butanol induced by the magnetic susceptibility. The samples were sealed in a glass sphere fitted into a 10 mm NMR tube to eliminate magnetic susceptibility corrections to the chemical shifts.[35] To improve sensitivity in ^{17}O NMR, ^{17}O-enriched water (11.10% $H_2{}^{17}O$, Cortecnet) was added to the solutions to yield approximately 1% ^{17}O enrichment. An acidified water solution ($HClO_4$, pH 3) was used as external reference. It was previously shown that an acidified water reference or the diamagnetic Zn^{2+} analogue of the Mn^{2+} complex measured at the same concentration and pH as the paramagnetic sample give identical results.[36] The temperature was varied between 271 and 358 K. It was calculated according to previous calibration with ethylene glycol and methanol.[37] Transverse relaxation times (T_2) were obtained by the Carr-Purcell-Meiboom-Gill spin-echo technique.[38] The ^{17}O NMR and NMRD data have been analysed according to the Solomon-Bloembergen-Morgan theory of paramagnetic relaxation applied to Mn^{2+} [39] using Visualiseur/Optimiseur running on a MATLAB 8.3.0 (R2014a) platform.

Computation Modelling

DFT calculations were performed using the ORCA 4.2 suite of programs.[40] Molecules were built using Avogadro software.[40-41] The integration grid was set to Lebedev 590 points with the final grid of Lebedev 770 points. The nature of each stationary point was characterized using frequency calculations. Geometry optimizations and free-energy calculations were performed at the PBE0/def2-SVP level of theory, with the Haywadt effective core potentials and LanL2DZ basis set for the metal ions. Solvation by water (ε = 80.2) was accounted for using the conductor-like polarizable continuum model (CPCM).[42] UCSF Chimera (version 1.14)[43] was used for the visualization of geometries and orbitals.

Essential Experimental Procedures/Data. ((All other characterization data, original spectra, etc., should be provided in the Supporting Information))

Acknowledgements

The authors thank the French Centre National de la Recherche Scientifique (CNRS) and the French National Research Agency (grant ANR-18-CE18-0008) for funding.

Keywords: manganese • bispidine • MRI contrast agents • complex stability • relaxometry

((References, please list all authors and do not use "et al."))

[1] T. Grobner, *Nephrol. Dial. Transplant.* **2006**, *21*, 1104-1108.
[2] E. Di Gregorio, G. Ferrauto, C. Furlan, S. Lanzardo, R. Nuzzi, E. Gianolio and S. Aime, *Invest. Radiol.* **2018**, *53*, 167-172.
[3] A. Gupta, P. Caravan, W. S. Price, C. Platas-Iglesias and E. M. Gale, *Inorg. Chem.* **2020**, *59*, 6648-6678.
[4] C. Andreini, I. Bertini, G. Cavallaro, G. L. Holliday and J. M. Thornton, *J. Biol. Inorg. Chem.* **2008**, *13*, 1205-1218.
[5] a) B. Drahoš, I. Lukeš and É. Tóth, *Eur. J. Inorg. Chem.* **2012**, *2012*, 1975-1986; b) M. Botta, F. Carniato, D. Esteban-Gomez, C. Platas-Iglesias and L. Tei, *Fut. Med. Chem.* **2019**, *11*, 1461-1483.
[6] M. Brandt, J. Cardinale, I. Rausch and T. L. Mindt, *J. Labelled Comp. Radiopharm.* **2019**, *62*, 541-551.
[7] D. Brasse and A. Nonat, *Dalton Trans.* **2015**, *44*, 4845-4858.
[8] S. Lacerda, D. Ndiaye and É. Tóth in *MRI relaxation agents based on transition metals*, *Vol. 78* Eds.: C. D. Hubbard and R. Van Eldik), **2021**, pp. 109-142.
[9] a) D. J. Erstad, I. A. Ramsay, V. C. Jordan, M. Sojoodi, B. C. Fuchs, K. K. Tanabe, P. Caravan and E. M. Gale, *Invest. Radiol.* **2019**, *54*, 697-703; b) E. M. Gale, I. P. Atanasova, F. Blasi, I. Ay and P. Caravan, *J. Am. Chem. Soc.* **2015**, *137*, 15548-15557; c) E. M. Gale, H.-Y. Wey, I. Ramsay, Y.-F. Yen, D. E. Sosnovik and P. Caravan, *Radiology* **2018**, *286*, 877-884; d) J. Wang, H. Wang, I. A. Ramsay, D. J. Erstad, B. C. Fuchs, K. K. Tanabe, P. Caravan and E. M. Gale, *J. Med. Chem.* **2018**, *61*, 8811-8824.
[10] a) R. Botár, E. Molnár, Z. Garda, E. Madarasi, G. Trencsényi, J. Kiss, F. K. Kálmán and G. Tircsó, *Inorg. Chem. Front.* **2022**, *9*, 577-583; b) R. Botár, E. Molnár, G. Trencsényi, J. Kiss, F. K. Kálmán and G. Tircsó, *J. Am. Chem. Soc.* **2020**, *142*, 1662-1666; c) F. K. Kálmán, V. Nagy, B. Váradi, Z. Garda, E. Molnár, G. Trencsényi, J. Kiss, S. Même, W. Même, É. Tóth and G. Tircsó, *J. Med. Chem.* **2020**, *63*, 6057-6065.
[11] a) Z. Garda, A. Forgács, Q. N. Do, F. K. Kálmán, S. Timári, Z. Baranyai, L. Tei, I. Tóth, Z. Kovács and G. Tircsó, *J. Inorg. Biochem.* **2016**, *163*, 206-213; b) G. A. Rolla, C. Platas-Iglesias, M. Botta, L. Tei and L. Helm, *Inorg. Chem.* **2013**, *52*, 3268-3279; c) Z. Garda, E. Molnár, F. K. Kálmán, R. Botár, V. Nagy, Z. Baranyai, E. Brücher, Z. Kovács, I. Tóth and G. Tircsó, *Front. Chem.* **2018**, *6*.
[12] https://clinicaltrials.gov/ct2/show/NCT05413668.
[13] A. M. Nonat, A. Roux, M. Sy and L. J. Charbonnière, *Dalton Trans.* **2019**, *48*, 16476-16492.
[14] D. Ndiaye, M. Sy, A. Pallier, S. Même, I. de Silva, S. Lacerda, A. M. Nonat, L. J. Charbonnière and É. Tóth, *Angew. Chem. Int. Ed.* **2020**, *59*, 11958-11963.
[15] M. Sy, D. Ndiaye, I. da Silva, S. Lacerda, L. J. Charbonniere, É. Tóth and A. M. Nonat, *Inorg. Chem.* **2022**, *61*, 13421-13432.
[16] P. Cieslik, P. Comba, B. Dittmar, D. Ndiaye, É. Tóth, G. Velmurugan and H. Wadepohl, *Angew. Chem. Int. Ed.* **2022**, *61*, e202115580.
[17] T. Siener, U. Holzgrabe, S. Drosihn and W. Brandt, *J. Chem. Soc. Perkin Trans. 2* **1999**, 1827-1834.
[18] A. Roux, A. M. Nonat, J. Brandel, V. Hubscher-Bruder and L. J. Charbonnière, *Inorg. Chem.* **2015**, *54*, 4431-4444.
[19] a) S. Aime, M. Botta, Z. Garda, B. E. Kucera, G. Tircso, V. G. Young and M. Woods, *Inorg. Chem.* **2011**, *50*, 7955-7965; b) G. Ferrauto, D. Delli Castelli, L. Leone, M. Botta, S. Aime, Z. Baranyai and L. Tei, *Chem. Eur. J.* **2019**, *25*, 4184-4193.
[20] P. Comba, U. Jermilova, C. Orvig, B. O. Patrick, C. F. Ramogida, K. Rück, C. Schneider and M. Starke, *Chem. Eur. J.* **2017**, *23*, 15945-15956.
[21] T. Legdali, A. Roux, C. Platas-Iglesias, F. Camerel, A. M. Nonat and L. J. Charbonnière, *J. Org. Chem.* **2012**, *77*, 11167-11176.

[22] R. Gillet, A. Roux, J. Brandel, S. Huclier-Markai, F. Camerel, O. Jeannin, A. M. Nonat and L. J. Charbonnière, *Inorg. Chem.* **2017**, *56*, 11738-11752.
[23] a) V. Haridas, S. Sadanandan, Y. K. Sharma, S. Chinthalapalli and A. Shandilya, *Tetrahedron Lettr.* **2012**, *53*, 623-626; b) S. Norrehed, M. Erdélyi, M. E. Light and A. Gogoll, *Org. & Biomol. Chem.* **2013**, *11*, 6292-6299.
[24] B. D. Hilton, G. N. Chmurny and G. M. Muschik, *J. Nat. Prod.* **1992**, *55*, 1157-1161.
[25] E. Toth, E. Brucher, I. Lazar and I. Toth, *Inorg. Chem.* **1994**, *33*, 4070-4076.
[26] a) K. Patel, A. Kumar and S. Durani, *BBA - Proteins and Proteomics* **2007**, *1774*, 1247-1253; b) M. Mori, E. Fumagalli, C. Castellano, A. Tresoldi, A. Sacchetti and F. Meneghetti, *Inorg. Chim. Acta* **2022**, *538*, 120968.
[27] H. Irving and R. J. P. Williams, *Nature* **1948**, *162*, 746-747.
[28] a) C. Vanasschen, E. Molnár, G. Tircsó, F. K. Kálmán, É. Tóth, M. Brandt, H. H. Coenen and B. Neumaier, *Inorg. Chem.* **2017**, *56*, 7746-7760; b) B. Drahoš, V. Kubíček, C. S. Bonnet, P. Hermann, I. Lukeš and É. Tóth, *Dalton Trans.* **2011**, *40*, 1945-1951.
[29] E. M. Gale, J. Zhu and P. Caravan, *J. Am. Chem. Soc.* **2013**, *135*, 18600-18608.
[30] H. E. Gottlieb, V. Kotlyar and A. Nudelman, *J. Org. Chem.* **1997**, *62*, 7512-7515.
[31] A. E. Martell and R. J. Motekaitis, *Determination and Use of Stability Constants*, VCH, Weinheim, **1992**, p.
[32] P. Gans, *Talanta* **2000**, *1*, 33-37.
[33] P. Gans, S. A. and A. Vacca, *Talanta* **1996**, *43*, 1739.
[34] R. M. Smith, R. J. Motekaitis and A. E. Martell in *NIST Standard Reference Database*, *Vol.* **1997**.
[35] A. D. Hugi, L. Helm and A. E. Merbach, *Helv. Chim. Acta* **1985**, *68*, 508-521.
[36] B. Drahos, J. Kotek, P. Hermann, I. Lukes and É. Tóth, *Inorg. Chem.* **2010**, *49*, 3224-3238.
[37] D. S. Raiford, C. L. Fisk and E. D. Becker, *Anal. Chem.* **1979**, *51*, 2050-2051.
[38] S. Meiboom and D. Gill, *Rev. Sci. Instrum.* **1958**, *29*, 688-691.
[39] E. Balogh, Z. He, W. Hsieh, S. Liu and É. Tóth, *Inorg. Chem.* **2007**, *46*, 238-250.
[40] F. Neese, *WIREs Computational Molecular Science* **2018**, *8*, e1327.
[41] M. D. Hanwell, D. E. Curtis, D. C. Lonie, T. Vandermeersch, E. Zurek and G. R. Hutchison, *J. Chemoinf.* **2012**, *4*, 17.
[42] J. Tomasi, B. Mennucci and R. Cammi, *Chem. Rev.* **2005**, *105*, 2999-3094.
[43] E. F. Pettersen, T. D. Goddard, C. C. Huang, G. S. Couch, D. M. Greenblatt, E. C. Meng and T. E. Ferrin, *J. Comput. Chem.* **2004**, *25*, 1605-1612.

Entry for the Table of Contents

Insert graphic for Table of Contents here. ((Please ensure your graphic is in **one** of following formats))

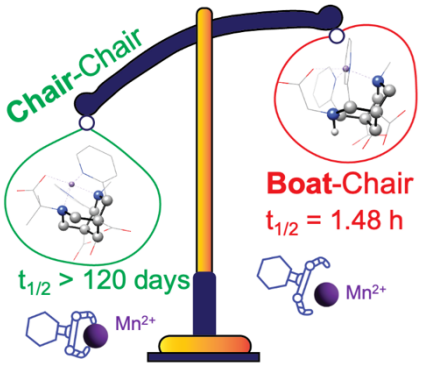

Mn(II) complexes with acetate-substituted bispidine ligands can adopt different conformations depending on the N3 substituent. Complexes in chair-chair conformation display high relaxivity and strong kinetic inertness, both very important for their potential use as MRI contrast agents. In contrast, the boat-chair conformers undergo fast dissociation and do no retain good relaxivity.